Materials Today Bio 28 (2024) 101254

Contents lists available at ScienceDirect

Materials Today Bio

journal homepage: www.journals.elsevier.com/materials-today-bio

Multifunctional vitamin D-incorporated PLGA scaffold with BMP/VEGF-overexpressed tonsil-derived MSC via CRISPR/Cas9 for bone tissue regeneration

So-Yeon Park [a,b,1], Jun-Kyu Lee [a,1], Sang-Hyeok Lee [a,1], Da-Seul Kim [a,b], Ji-Won Jung [a], Jun Hyuk Kim [a], Seung-Woon Baek [a], Seungkwon You [c,*], Dong-Youn Hwang [a,**], Dong Keun Han [a,***]

[a] Department of Biomedical Science, CHA University, Gyeonggi-do, 13488, Republic of Korea
[b] Division of Engineering in Medicine, Department of Medicine, Harvard Medical School, Brigham and Women's Hospital, Cambridge, MA, 02139, USA
[c] Division of Biotechnology, College of Life Sciences and Biotechnology, Korea University, Seoul, 02841, Republic of Korea

ARTICLE INFO

Keywords:
CRISPR Cas9
Vitamin D
PLGA scaffold
BMP2/VEGF-Overexpression
Tonsil-derived MSC

ABSTRACT

Guiding endogenous regeneration of bone defects using biomaterials and regenerative medicine is considered an optimal strategy. One of the effective therapeutic approaches involves using transgene-expressed stem cells to treat tissue destruction and replace damaged parts. Among the various gene editing techniques for cells, clustered regularly interspaced short palindromic repeats (CRISPR)/CRISPR-associated protein 9 (Cas9) is considered as a promising method owing to the increasing therapeutic potential of cells by targeting specific sites. Herein, a vitamin D-incorporated poly(lactic-co-glycolic acid) (PLGA) scaffold with bone morphogenetic protein 2 (BMP2)/vascular endothelial growth factor (VEGF)-overexpressed tonsil-derived MSCs (ToMSCs) via CRISPR/Cas9 was introduced for bone tissue regeneration. The optimized seeding ratio of engineered ToMSCs on the scaffold demonstrated favorable immunomodulatory function, angiogenesis, and osteogenic activity *in vitro*. The multifunctional scaffold could potentially support stem cell *in vivo* and induce the transition from M1 to M2 macrophage with magnesium hydroxide and vitamin D. This study highlights the improved synergistic effect of a vitamin D-incorporated PLGA scaffold and a gene-edited ToMSCs for bone tissue engineering and regenerative medicine.

1. Introduction

Critical-sized bone defects caused by trauma, surgical tumor resection, or infection are defined as those that do not heal naturally within a specific period. While Autologous bone grafts are a viable treatment opinion for these defects, their clinical application is restricted by issues such as donor site morbidity, limitation of source, and potential immunity risks. To restore the bone defect to its original structures and function, various synthetic materials have been investigated, including ceramics, plastic glasses, calcium compounds, and bioresorbable substances [1–3]. Although metal scaffolds are chosen for their robust mechanical support and stability, they can lead to long-term complications, such as stress shielding and local inflammation. Synthetic polymer-based scaffolds have the potential to optimize drug distribution and release kinetics, promoting bone tissue regeneration and repair. In our recent research, poly(lactide-co-glycolide) (PLGA) along with magnesium hydroxide (MH) was served as a porous composite scaffold to support cells [4–6]. Vitamin D3 (VD) is a fat-soluble vitamin that plays a crucial role in regulating calcium metabolism as a steroid hormone. Clinical studies have demonstrated that VD administration and topical application can enhance osteointegration rates and various tissue engineering [7,8].

Compared to being on medication, stem cell-based therapy has shown promising results for various tissue injuries. Mesenchymal stem

* Corresponding author.
** Corresponding author.
*** Corresponding author.
E-mail addresses: bioseung@korea.ac.kr (S. You), hdy@cha.ac.kr (D.-Y. Hwang), dkhan@cha.ac.kr (D.K. Han).
[1] These authors contributed equally to this work.

https://doi.org/10.1016/j.mtbio.2024.101254
Received 24 July 2024; Received in revised form 8 September 2024; Accepted 14 September 2024
Available online 14 September 2024

cells (MSCs) are extensively studied for their multipotent differentiation capabilities and paracrine effects. However, their clinical translation and application have several limitations, such as issues with immunosuppression and undefined differentiation lineages *in vivo*. ToMSCs, generally obtained from tonsillectomies, have emerged as attractive MSCs for clinical applications owing to their stable supply, noninvasive acquirement process, and high proliferation rate [9,10].

To enhance the therapeutic effect of ToMSCs, the expression of one or more transgenes has been used [11]. Among the various genetic engineering techniques available, the RNA-guided CRISPR/Cas9 nuclease system has risen as the leading genome engineering technology due to its cost-effectiveness, time efficiency, labor-saving attributes, high efficacy, and precision [12,13]. Over the past decade, knock-in of various genes has been attempted to improve the effectiveness of gene therapy. Bone morphogenetic proteins (BMPs) are an important class of growth factors that play a central role in most ossification processes. Among the BMPs, bone morphogenetic protein 2 (BMP2) has shown superior osteogenic initiation capabilities for complete bone formation

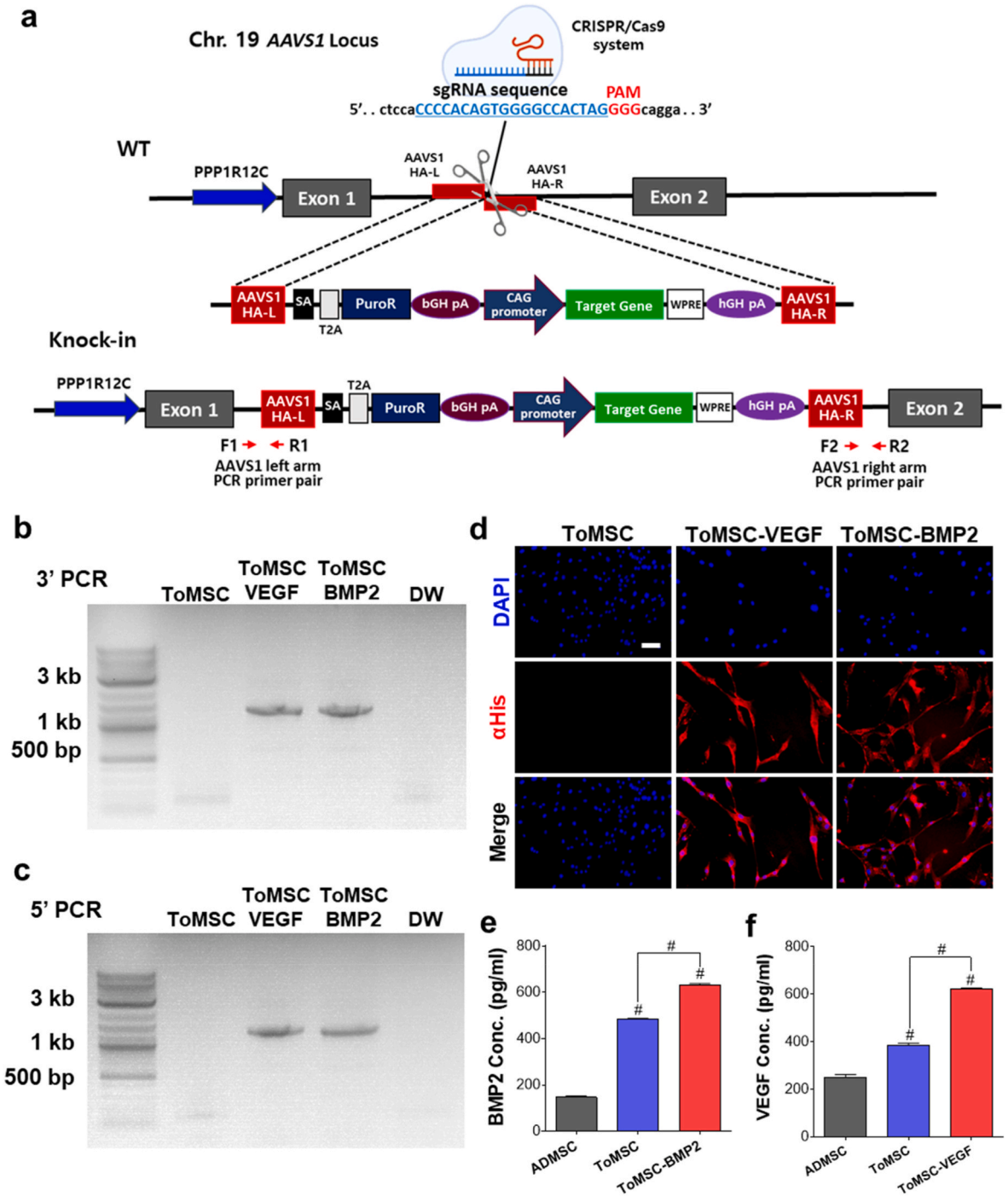

Fig. 1. Characterization of CRISPR/Cas9-edited ToMSC lines. (a) Schematic representation of CRISPR/Cas9-mediated transgene knock-in process. (b, c) Confirmation of successful on-target knock-in by analyzing the genomic sequences through genomic PCR, utilizing primer pairs F1/R1 (top) and F2/R2 (bottom). (d) Immunostaining to detect the expression of VEGF and BMP2 originating from the transgenes. To differentiate transgene-derived proteins from their endogenous counterparts, antibodies targeting the His-tag were employed for immunostaining. Quantitative assessment of total protein levels of BMP2 (e) and VEGFA (f) using ELISA. #$p < 0.0001$, ***$p < 0.001$, **$p < 0.01$, and *$p < 0.05$ indicate statistically significant differences, respectively.

in numerous studies [14,15]. In most tissue regeneration processes with the exception of cornea or cartilage, angiogenesis is regarded as an essential prerequisite due to its role in providing necessary nutrients, transporting macromolecules, and maintaining the microenvironment [16]. Therefore, the transfer of two pivotal genes, vascular endothelial growth factor (VEGF) for angiogenesis and BMP2 for osteogenesis, into ToMSCs enhances the potential for tissue regeneration and successfully achieves bone repair. In this study, the functions and advantages of genetically engineered cells were validated by assessing their impact on bone regeneration, vascular regeneration, and M2 polarization depending on the presence or absence of cells on the scaffolds. The utilization of a multifunctional VD-incorporated PLGA/MH scaffold (PMEV), combined with BMP/VEGF-overexpressed tonsil-derived MSC using CRISPR/Cas9, holds promise for enhancing bone tissue engineering.

2. Results

2.1. CRISPR/Cas9-mediated knock-in of BMP2 and VEGF genes into ToMSCs

FACS analysis demonstrated the expression of CD44, CD73, CD90, CD105, HLA-DRB1, and HLA-ABC in ToMSCs (Supplementary Fig. 1). To confirm the multipotency of the isolated ToMSCs, they were differentiated into various cell lineages, including adipocytes, osteocytes, and chondrocytes compared to adipose-derived MSCs (ADMSCs) as a control

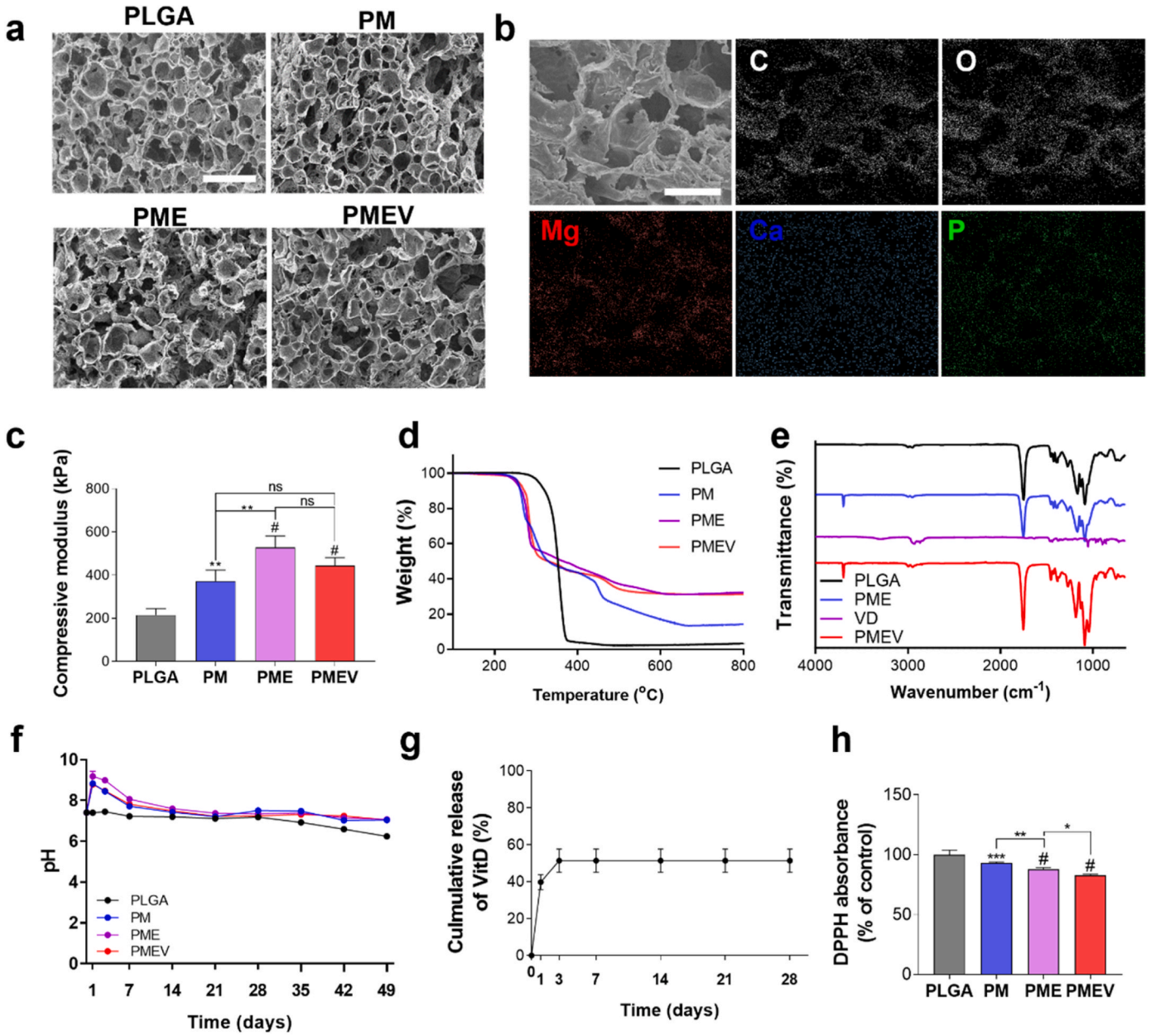

Fig. 2. Characterization of the scaffolds: (a) Visualization of the scaffold surface morphology using scanning electron microscopy (SEM, scale bar = 500 μm); MH-incorporated PLGA scaffold (PM). (b) Elemental mapping of the PMEV scaffold using field emission-SEM equipped with energy dispersive spectroscopy (scale bar = 200 μm). (c) Compressive modulus of the scaffolds using universal testing machine. (d) Assessment of thermal properties of each scaffold using a thermogravimetric analyzer. (e) FTIR spectra of the scaffold on 600–4000 cm^{-1}. (f) Monitoring of the pH value during the degradation process of the scaffold in 400 μl PBS solution for 49 days. (g) The release profile of VD from the scaffold using HPLC with C18 reverse column. (h) DPPH absorbance in each scaffold. #$p < 0.0001$, ***$p < 0.001$, **$p < 0.01$, and *$p < 0.05$ indicate statistically significant differences, respectively.

(Supplementary Fig. 2). ToMSCs exhibited superior differentiation ability in osteogenesis and chondrogenesis while showing low adipogenic differentiation. The BMP2 and VEGF genes, known for their substantial contributions to osteogenesis, were integrated into the AAVS1 locus, a well-known safe-harbor site on the chromosome via CRISPR/Cas9-mediated homology-directed repair (HDR) (Fig. 1a). On-site knock-in via HDR of the transgene-containing donor DNA was examined through genomic DNA PCR using two primer pairs (F1/R1 for 5′end and F2/R2 for 3′end of the inserted DNA), as shown in Fig. 1a. The PCR fragments of the expected size (1176 and 1128 bp, respectively) indicated successful on-site insertion (Fig. 1b and c). The expression of BMP2 and VEGFA from the introduced transgenes was confirmed through immunocytochemistry (ICC). An antibody specific to the His tag exclusively detected BMP2 and VEGFA expression originated from the BMP2-6His transgene, not from the endogenous BMP2 gene (Fig. 1d). ELISA revealed that the total protein levels of BMP2 and VEGFA secreted from ToMSC-BMP2 and ToMSC-VEGF were approximately 1.3- and 1.6-fold higher, respectively, compared to ToMSC (Fig. 1e and f). The modest increase in total proteins observed in ToMSC-BMP2 and ToMSC-VEGFA, in contrast to ToMSC, can be attributed to the inherent high-level expression of these proteins in ToMSC when compared to ADMSCs. Osteogenic differentiation was conducted to compare the mineralization of engineered ToMSCs to ADMSCs and normal ToMSCs (Supplementary Fig. 3). The results indicated that ToMSC-BMP2 and ToMSC-VEGF displayed enhanced osteogenic differentiation capacity. Therefore, it is anticipated that the BMP2 and VEGF transgenes have a positive effect on osteogenesis.

2.2. Scaffold characterization

The freeze-drying method is a technology used to fabricate highly porous 3D scaffolds with porogens, including natural polymers, synthetic polymers, and ceramics for bone tissue regeneration. In this study, PLGA was selected as the matrix of the scaffold for delivering cells and drugs. The scaffolds exhibited a randomly distributed pores with sizes ranging from 200 to 300 μm, as observed using SEM and quantified through ImageJ software (Fig. 2a and Supplementary Fig. 4).

The minimum pore diameter required for bone tissue growth has been reported to be 50–100 μm [17]. Smaller pore sizes have been shown to aid osteoblast attachment but interfere with nutrient transport and blood vessel formation. Studies of various materials have reported that a pore size of 300 μm induces bone formation with a strength similar to that of natural bone [18]. Elemental mapping was conducted to verify the arrangement and distribution of magnesium, calcium, and phosphorous within the PMEV scaffold (Fig. 2b). The effect of MH and ECM addition on the mechanical properties of porous PLGA scaffolds was analyzed using compression tests (Fig. 2c and Supplementary Fig. 5). The incorporation of each component except for VD, led to an increase in the compressive modulus to 215.2, 371.5, 527.3, and 442.6 kPa, respectively. The addition of MH contributed to the increase in compressive modulus due to its ceramic nanoparticle composition, which provides additional structural reinforcement. Similarly, the ECM enhanced the mechanical properties, as its inorganic components help to further strengthen the scaffold by mimicking the natural bone extracellular matrix. The inorganic composition of the scaffold was measured using TGA (Fig. 2d). Both PME and PMEV exhibited similar final values of approximately 32 %, while PM showed 16 % of the remaining mass. FTIR spectrometer was employed to confirm the presence of VD in the scaffold (Fig. 2e and Supplementary Fig. 6). PMEV had the free -CH_3 stretching peak of VD unlike PLGA and PME, confirming presence of VD in the PMEV scaffold. Porosity measurements using a mercury porosimeter showed no significant differences (Supplementary Fig. 7). To investigate the pH neutralization ability of MH and the release of VD, the degradation experiment was executed. The scaffolds were immersed in a PBS solution at 37 °C for 49 days with light shaking. During the degradation of PLGA, hydrolytic byproducts were released, resulting in an acidic microenvironment with low pH around the implant [19]. While the pH of PLGA decreased to 6.23, the groups containing MH maintained a pH level consistent with physiological conditions (Fig. 2f). It demonstrated that the MH could neutralize the acidic byproducts of the PLGA. In the release profile, about 50 % of VD was released within 3 days and reached a plateau (Fig. 2g). Recent studies have proved the presence of VD receptors in activated macrophages and lymphocytes, activating antimicrobial genes and suppressing the expression of pro-inflammatory cytokines for anti-inflammation [20]. The early release of VD suppresses inflammation through ROS inhibition and enhances early bone formation. Oxidative stress, cell damage, and inflammation characterized by mass radicals in the wound area, were examined using a DPPH assay to investigate the antioxidant activity of MH and VD on the scaffolds [21,22]. All scaffolds exhibited significant radical scavenging effects on DPPH compared to PLGA. After 1 h of incubation, PM, PME, and PMEV displayed lower DPPH absorbance value of 93.2 %, 87.5 %, and 82.7 %, respectively compared to the Control (Fig. 2h). The anti-inflammatory capacity of PMEV was demonstrated through the analysis of pH neutralization and ROS scavenging ability of MH and VD, respectively.

2.3. Macrophage polarization

Macrophage polarization plays a central role in directing tissue regeneration post-injury. Depending on various stimuli, macrophages can transit into either inflammatory (M1) or anti-inflammatory (M2) phenotypes [23,24]. RAW 264.7, murine macrophages, were treated with LPS and IFN-γ to induce M1 macrophages. To evaluate the impact of a VD-incorporated scaffold on M2 polarization, the transformation of macrophage status from M1 to M2 was first investigated by ICC (Fig. 3a). Notably, the PME and PMEV scaffolds exhibited an intense red signal for Arg1 (M2 phenotype), indicating enhanced activation of M2 macrophage in response to ECM and VD. We attributed this outcome to the immunomodulatory effect of VD on the scaffold through ROS scavenging ability. D-Lactide interaction with TLR2 and/or TLR9 on macrophages induced suppression of the PI3K/Akt pathway and activation of the NF-κB pathway, facilitating the transition from M2 to M1 [25]. The macrophage polarization was assessed using FACS (Fig. 3b and c). When gated on the M1 marker CD86 and M2 marker CD206, we observed an increase in CD206-positive cells and a decrease in CD86-positive cells on the PMEV scaffolds compared to PLGA. Moreover, PLGA demonstrated the highest expression of inflammatory macrophage. This M1/M2 polarization trend implies that the addition of MH and VD on the PLGA scaffold could affects the immune modulation of macrophages by suppressing ROS production and neutralizing lactide from PLGA. Polarized macrophages secrete various types of cytokines for regulating inflammation and disease and are vital for differentiation and survival. Interleukin 10 (IL-10) is a potent anti-inflammatory cytokine that inhibits immune proliferation and bone resorption [26]. On the contrary, IL-6 is a key inflammatory cytokine-induced in the early stages by activating the STAT3 signaling pathway [27]. In RT-qPCR, the expression of IL-6 was highest in PLGA, and the MH-containing groups inhibited its expressions. Moreover, the VD-incorporated scaffold showed a significant difference in two cytokines compared to the MH-containing groups (Fig. 3d and e). Based on the immune-reprogramming ability of the scaffold, the PMEV was adopted as a main scaffold for further *in vitro* and *in vivo* analysis with gene edited-ToMSCs.

2.4. Angiogenic effect of PMEV/BV

In this study, we aimed to achieve complete bone tissue regeneration using two types of gene-edited ToMSCs targeting BMP2 and VEGF. The ideal cell combination ratio was optimized by conducting tube formation assay with HUVECs and assessing osteogenic differentiation in MC3T3-E1 cells to enable efficient treatment with both types. A

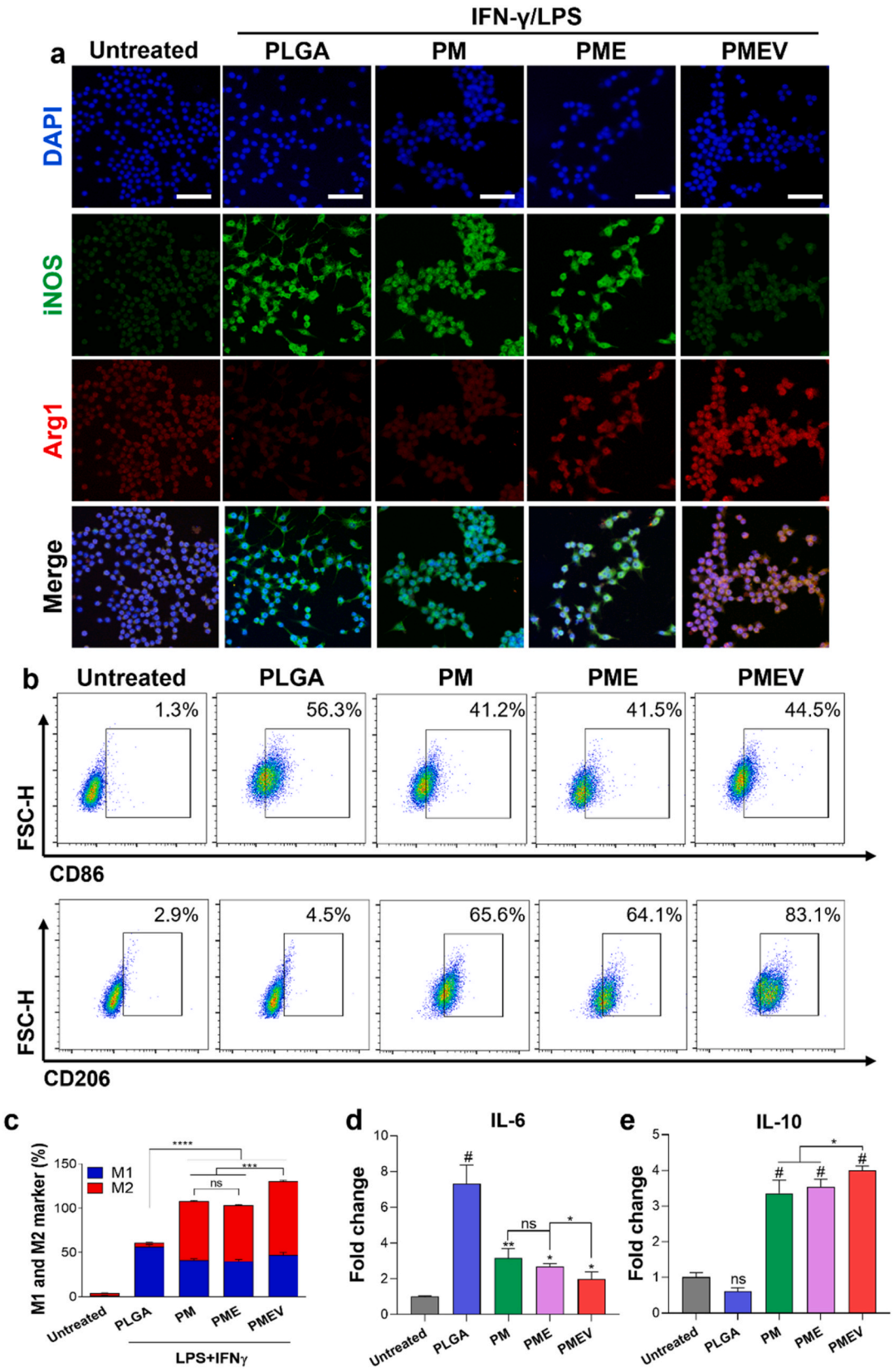

Fig. 3. M1/M2 polarization capacity of the scaffolds: (a) Immunocytochemistry of RAW264.7 cells exposed to M1 inducing factors, IFN-γ and LPS, in the presence of each scaffold (DAPI: blue, iNOS: green, Arg1: red; scale bar = 50 μm). (b) Flow cytometry dot plot illustrating activation markers on $CD86^+$ and $CD206^+$ macrophages. (c) Quantification of polarized M1 and M2 macrophages expressing CD86 and CD206, respectively. (d) Analysis of mRNA expression levels for IL-6 and IL-10. #$p < 0.0001$, ***$p < 0.001$, **$p < 0.01$, and *$p < 0.05$ indicate statistically significant differences, respectively. (For interpretation of the references to color in this figure legend, the reader is referred to the Web version of this article.)

comparison between single and dual types of cells using a hanging insert, without the use of a scaffold, demonstrated that the optimal composition for promoting angiogenesis and osteogenesis was a 2:1 ratio (ToMSC-BMP2:ToMSC-VEGF) (Supplementary Figs. 8 and 9). All experiments from this point on were performed with PMEV scaffolds containing two types of cells in a 2:1 ratio (PMEV/BV).

To assess the angiogenic effects of VD-incorporated scaffolds and VEGF-overexpressed ToMSCs, we conducted tube formation assays on Matrigel matrices. This comprehensive analysis of multiple cellular-activated processes, including cell migration, cell-cell interaction, survival, and apoptosis. The PLGA scaffold exhibited the smallest tubular structures and discontinued network, whereas the scaffolds with MH and VD displayed longer tube lengths and branch points compared to PLGA, especially in the PMEV/BV (Fig. 4a and b). According to the results and the other study, PLGA reduced cell permeability and migration ability, resulting in EC dysfunction [28]. The angiogenic gene expression was also confirmed using RT-qPCR at day 3 (Fig. 4c). Gene upregulation in PMEV/BV suggested that the angiogenic pathway was activated by the scaffolds and ToMSCs. In all gene expressions including VEGF, fibroblast growth factor 2 (FGF2), angiopoietin 1 (ANG1), and hepatocyte growth factor (HGF), a similar upregulation trend was exhibited compared to results of the tube formation assay. Since the phenomenon that VD and engineered stem cells could induce endothelial cell proliferation and migration is observed, the relevant molecular signaling cascades were analyzed to confirm the mechanism of promoted angiogenesis using western blotting. At a predetermined time points, HUVECs were harvested and lysed for the verification of VEGFR2 signaling activation. In cases of increased VEGF activation, PI3K/Akt and MEK/ERK signals play a pivotal role in vasculogenesis [29,30]. It is well established that phosphorylated ERK and Akt are key downstream components of the Ras/Raf/MEK and PI3K/Akt/mTOR pathways, respectively [31,32]. Our investigation into the effects of ToMSCs-VEGF on stimulating ERK and Akt phosphorylation (Fig. 4d and e) revealed that VEGF-overexpressed ToMSCs highly expressed downstream signaling through the VEGFA/VEGFR2 pathway, reaching peak activation at 90 min post-treatment. These results suggest that ToMSCs-VEGF

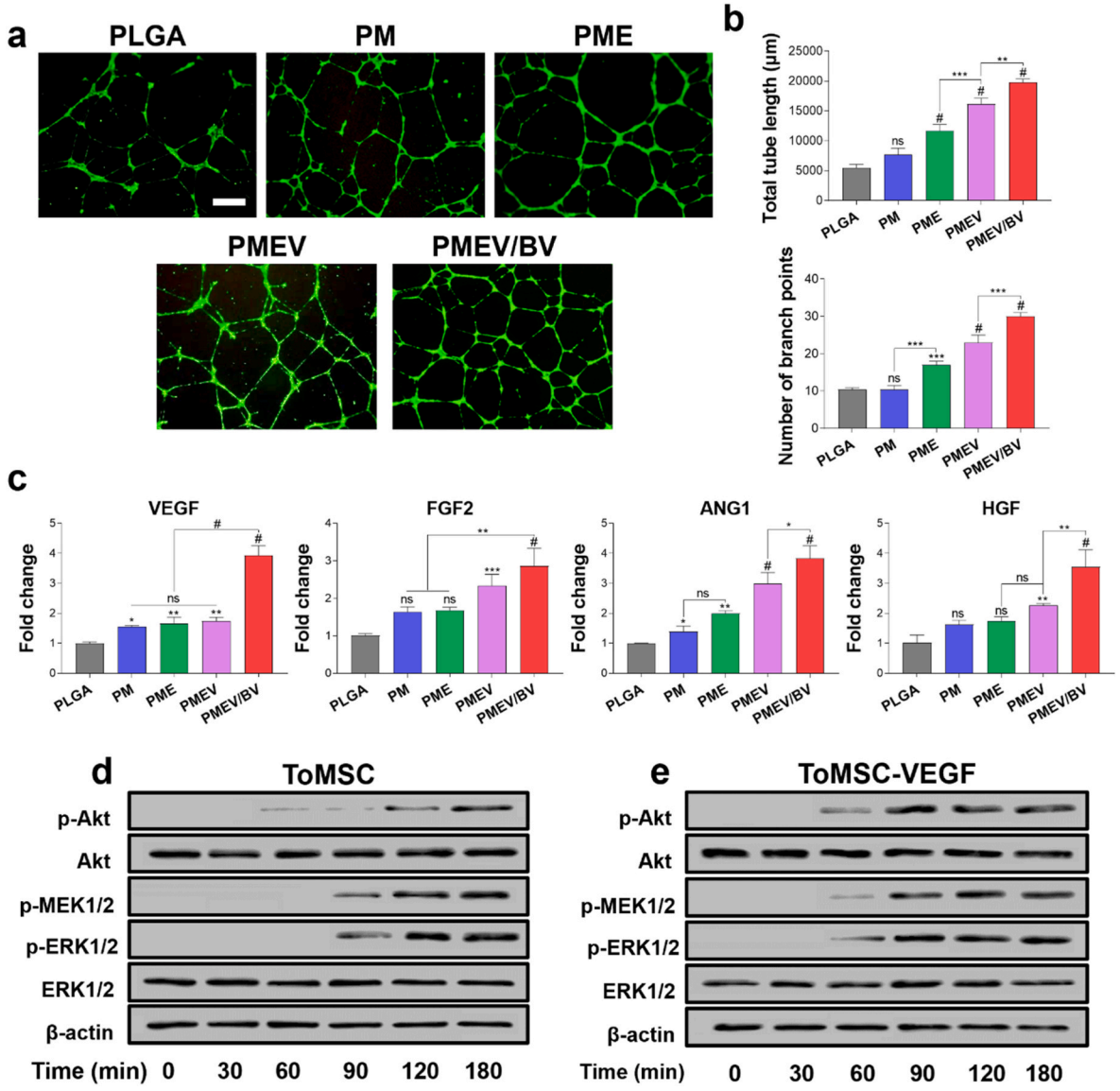

Fig. 4. Angiogenic effect of the engineered-ToMSC with the scaffold: (a) Representative stained images from the tube formation assay (scale bar = 500 μm). (b) Quantification of the tube network, including total tube length and the number of branch points. (c) Evaluation of mRNA expression related to angiogenesis, including VEGF, FGF2, ANG1, and HGF using RT-qPCR. (d, e) Western blot analysis for time-dependent expression of the VEGF/VEGFR2 signaling pathway in HUVECs with ToMSCs-seeded scaffold over 0–180 min. β-actin was used as a loading control. #$p < 0.0001$, ***$p < 0.001$, **$p < 0.01$, and *$p < 0.05$ indicate statistically significant differences, respectively.

when seeded on the scaffold, can robustly regulate VEGF-related intracellular signaling pathways.

2.5. Osteogenic differentiation with PMEV/ToMSC-BV

To assess the osteogenic potential of the scaffold in combination with ToMSCs, the MC3T3-E1 cells, murine pre-osteoblasts, were co-cultured in an osteogenic differentiation medium beneath a hanging insert. It is widely accepted that the early marker of osteogenesis is ALP which can regulate the formation of calcium phosphate on the ECM [33]. The production of ALP was assessed using ALP staining and activity assay kit after 7 days of differentiation (Fig. 5a and b). The images and quantitative results demonstrated that PMEV/BV significantly enhanced the early stages of osteogenic differentiation compared to group without cells. For further evaluation of *in vitro* osteogenic characteristics of the scaffolds, ARS staining was also conducted on MC3T3-E1 cells at 21 days. Similarly, the highest calcium deposition was observed in the PMEV/BV compared to all other groups (Fig. 5c and d). The mRNA expression related to osteogenesis, including ALP, runt-related transcription factor 2 (RUNX2), osteocalcin (OCN), and osterix (OSX) was also evaluated (Fig. 5e). The presence of both VD and ToMSCs on the scaffold significantly upregulated the expression levels of osteogenic markers on day 7, indicating accelerated maturation of osteoblast *in vitro*. The expression of OSX, an essential transcription factor for osteoblast differentiation, showed significant differences across all groups compared to PLGA. Transforming growth factor-beta (TGF-β)/BMP regulates osteogenesis through the activation of receptor serine/threonine kinases [34]. The underlying mechanism of the BMP2 signaling pathway was determined by comparing ToMSCs and ToMSC-BMP2 using western blotting (Fig. 5f, g and Supplementary Fig. 10). MC3T3-E1 cells were harvested at different time points and lysed to analyze the activation kinetics of RUNX2. Maximum RUNX2 in ToMSC occurred at 120 h, respectively. ToMSC-BMP2 exhibited more saturated expression compared to ToMSC at 72 h. These results of align with those observed in the angiogenic signaling pathway, highlighting that the presence of engineered-ToMSCs can induce *in vitro* osteogenic differentiation. Evaluation of angiogenesis and osteogenesis revealed that the incorporation of engineered ToMSCs onto scaffolds significantly upregulated several functions, including osteogenesis, angiogenesis, and anti-inflammation.

2.6. In vivo angio-osteogenesis

Most tissues rely on blood vessels to supply nutrients and oxygen to every cell [35]. Insufficient vascularization can result in improper cell integration or cell death during tissue-engineered regeneration. When tissue grows beyond a length of 100–200 μm, the formation of new blood vessel becomes crucial. To assess vascularization at the defect site, micro-CT was utilized using an opaque compound under physiological pressure. The quantified results revealed that PMEV/BV exhibited the development of newly formed, thick vessels, and it showed statistically no difference with the Native (Fig. 6a and b). In contrast, PLGA and

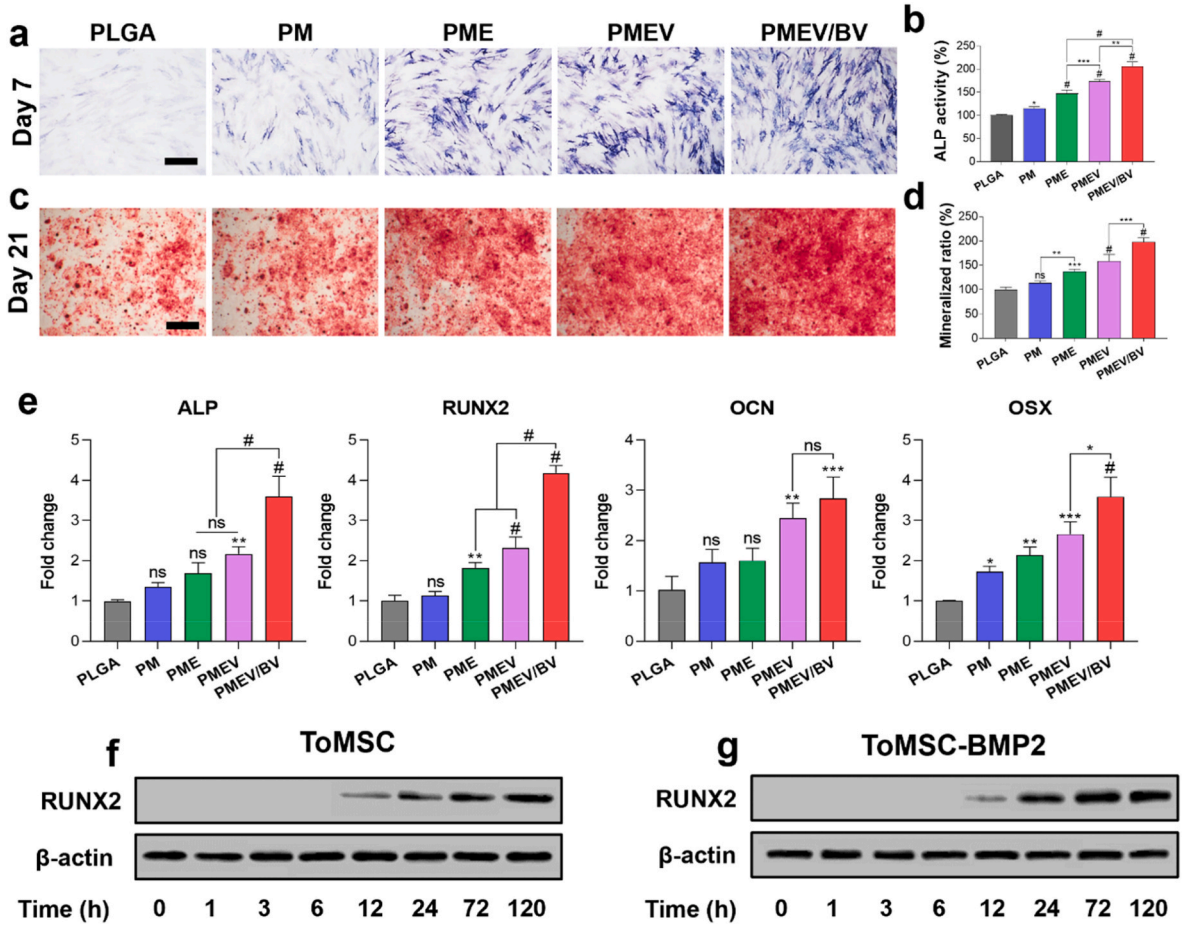

Fig. 5. Osteogenic ability of the engineered-ToMSC with the scaffold *in vitro*: (a) Representative ALP staining images with each scaffold at 7 days of osteogenic differentiation (scale bar = 500 μm). (b) Quantification of ALP activity. (c) Representative ARS staining images with each scaffold at 21 days of osteogenic differentiation (scale bar = 500 μm). (d) Quantification of mineralized ratio. (e) Osteogenesis-related gene expression with the scaffolds was analyzed using RT-qPCR at 21 days. (f, g) Western blotting for time-dependent expression of RUNX2 in MC3T3-E1 with ToMSC-seeded scaffold over 0–120 h #$p < 0.0001$, ***$p < 0.001$, **$p < 0.01$, and *$p < 0.05$ indicate statistically significant differences, respectively.

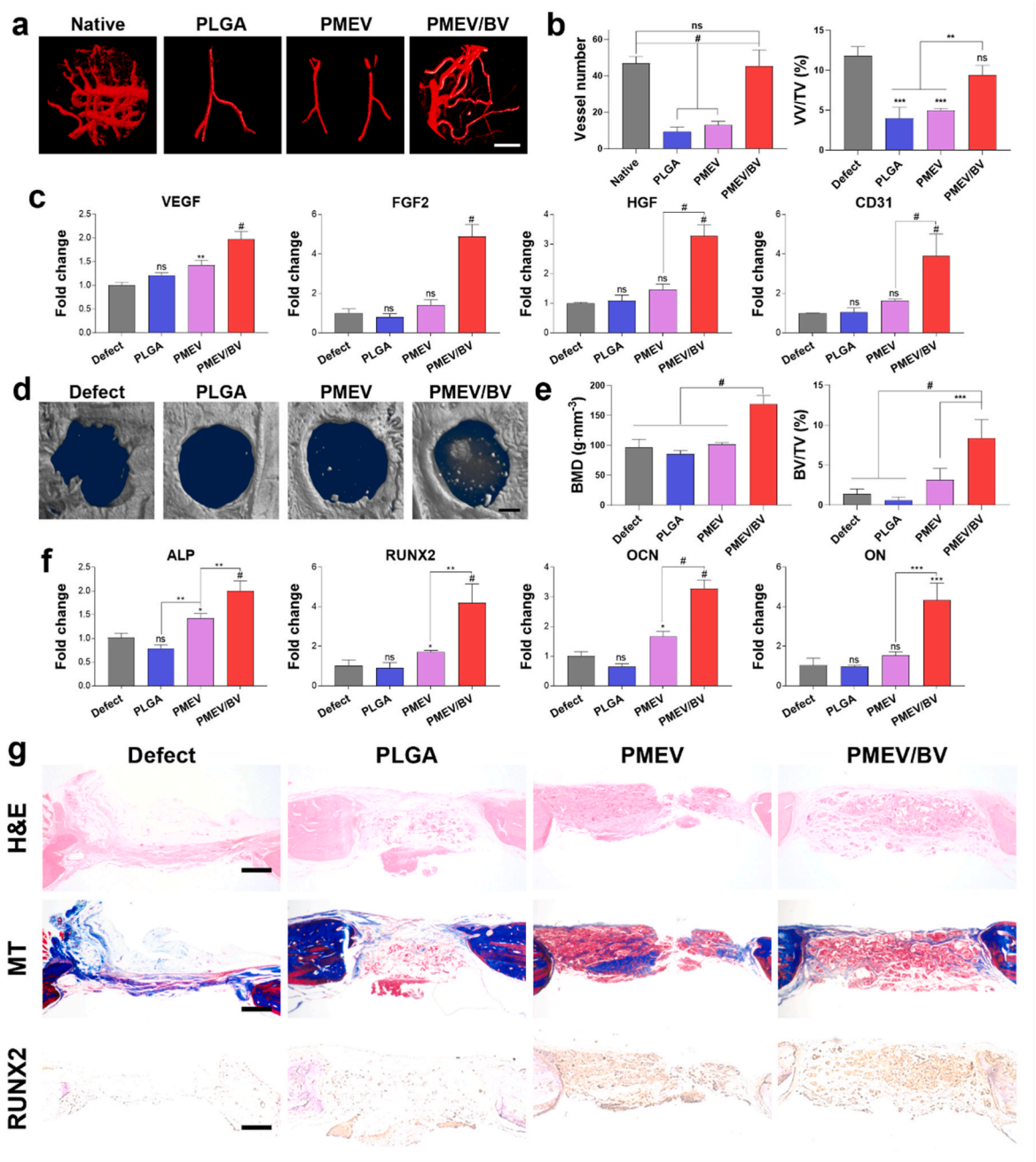

Fig. 6. Vascularization and osteogenesis of PMEV/BV on rat calvaria defect: (a) 3D reconstruction images of the vasculature (red) at 8 weeks post-implantation (scale bar = 1000 μm). (b) Quantification of vascularization on vessel number and vessel volume density. (c) Expression of mRNA-related to angiogenesis using RT-qPCR for VEGF, FGF2, HGF, and CD31. (d) Representative micro-CT images of rat calvaria with mineralized new bone at 8 weeks post-implantation (scale bar = 1000 μm). (e) Quantification of bone mineral density and bone volume density. (f) Expression of mRNA-related to osteogenesis using RT-qPCR for ALP, RUNX2, OCN, and ON. (g) Histological analysis with H&E, MT, and IHC for RUNX2 (scale bar = 100 μm). (For interpretation of the references to color in this figure legend, the reader is referred to the Web version of this article.)

PMEV showed fewer and thinner vessels. Gene expression analysis, including VEGF, FGF2, HGF, and CD31, also indicated enhanced angiogenesis in the ToMSCs-incorporated groups. PMEV/BV showed significant differences in all genes compared to all other groups, including PMEV (Fig. 6c). A new bone formation at the defect site after 8 weeks of implantation was investigated using micro-CT (Fig. 6d and e). In the micro-CT images, the defects in PLGA and PMEV remained largely open with minimal mineralized new bone at regions at the edges. PMEV/BV exhibited more extensive bone growth and mineralized areas at the center of the defect driven by the gene-edited ToMSCs. The relatively higher BMD values observed in the final group are likely due to the early stages of bone regeneration, where fine bone structures are forming from the center of the tissue. These newly formed bones in the micro-CT images contribute to the increased BMD values. However, the absolute BMD values remain lower compared to those reported in previous studies. Furthermore, similar findings can be observed in the histological analysis, where the formation of fine bone structures from the center is evident. Relative mRNA expression of ALP, RUNX2, OCN, and ON was calculated using RT-qPCR (Fig. 6f). Histological analysis was also conducted to support the radiological findings further and to confirm the mineralization. The sagittal section was stained with H&E and MT, consistently revealing newer and more collagen tissue with

dense distribution in PMEV/BV. MT staining indicated that the regenerated bone, with collagen fibers (blue) and mature bone (red), was observed. MT expression shows that the bone was regenerated using a scaffold. Moreover, RUNX2 staining demonstrated a higher expression of osteogenic markers in the PMEV/BV group, indicating enhanced bone formation. PMEV/EV group exhibited a thicker and denser mature bone tissue morphology compared to the defect group, which shows naturally regenerated bone in a portion of the damaged tissue.

Long-term BMP-2 activity within the defect area has been reported to promote bone formation more efficiently than short-term activity [36]. Therefore, reliable, sustained, and local delivery of bioactive BMP2 to the defect site is important for successful bone repair. The immunohistochemical staining of RUNX2 was performed to confirm whether BMP2 delivered over a long period of time from ToMSC-BMP2 was clearly

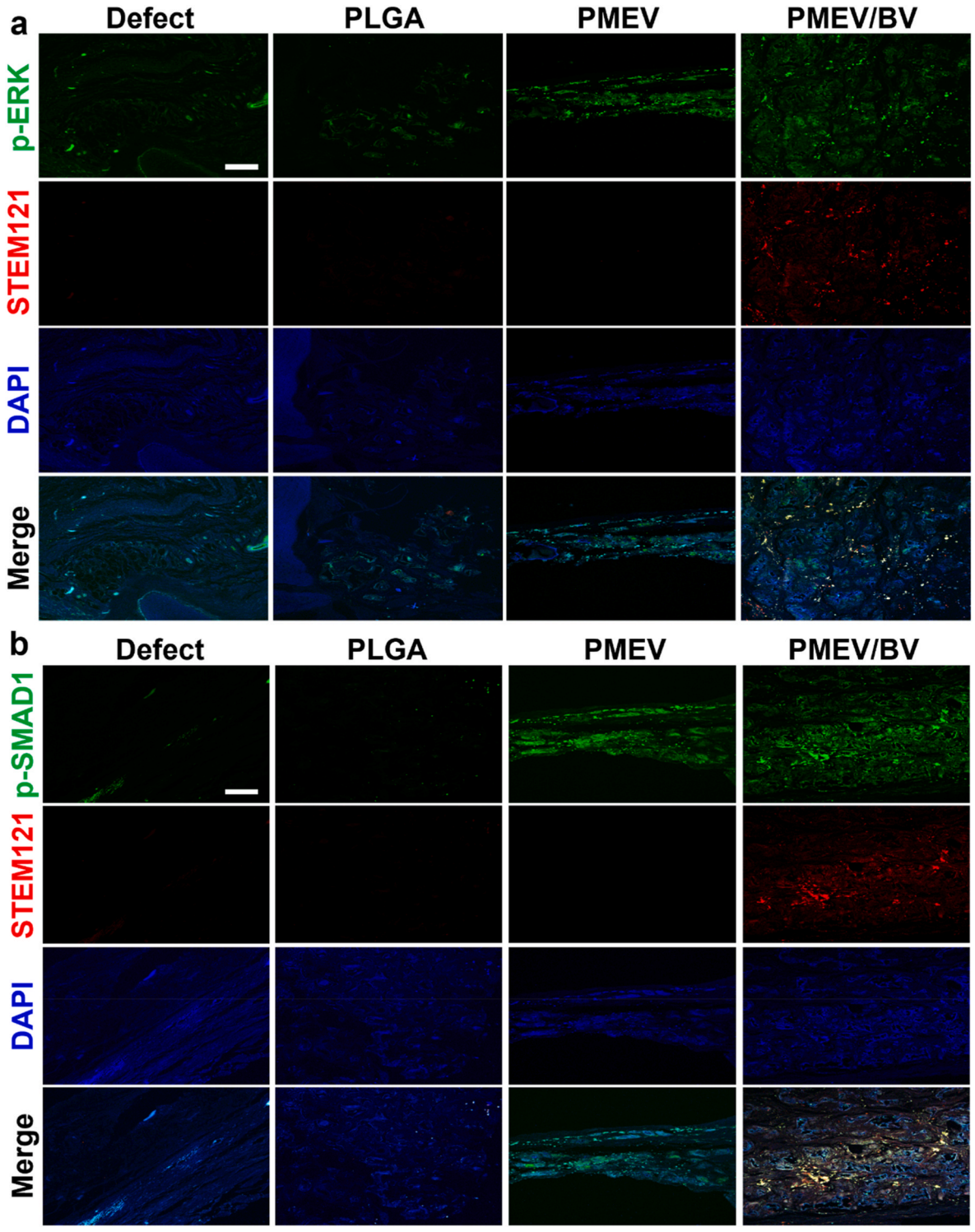

Fig. 7. Histopathological analysis of the gene-edited ToMSCs-seeded scaffold after 8 weeks using human specific marker and BMP2/VEGF signaling molecules. (a) Immunofluorescence image of rat calvaria at 8 weeks on p-ERK (green), STEM121 (red), and DAPI (blue); scale bar = 100 μm. (b) Immunofluorescence image of rat calvaria at 8 weeks for p-SMAD1/5/8 (green), STEM121 (red), and DAPI (blue); Scale bar = 100 μm. (For interpretation of the references to color in this figure legend, the reader is referred to the Web version of this article.)

involved in the subsequent osteogenesis process. The deposition of osteogenic proteins was observed at the defect region of both PMEV and PMEV/BV. These results suggest that the PMEV/BV acts as a bone regenerative therapy, promoting *in situ* bone tissue regeneration without any cell leakage.

2.7. Histopathological finding for transplantation of ToMSCs-seeded PMEV/BV

The expression levels of inflammation-related genes, IL-6 and IL-10 were quantified using RT-qPCR. In IL-6, the MH-containing group exhibited inhibition of its expression, whereas the anti-inflammatory cytokine was enhanced in the PMEV and PMEV/BV (Supplementary Fig. 11). *In vivo* inflammation was also regulated by the M1/M2 polarization of macrophages through VD of the scaffold. To assess the distribution of transplanted cells, immunostaining was performed 8 weeks post-transplantation. STEM121 specifically reacts with a human cytoplasmic marker, visualizing engraftment, migration, and differentiation of human cells in mice and rats. Transplanted cells, identified by the human cell marker STEM121 (Y40410, Taraka), were widely distributed in the PMEV/BV (Fig. 7a and b). p-ERK1/2 and p-SMAD1/5/8, downstream signaling molecules of VEGF and BMP2, were also labeled as markers of tissue regeneration. In the Defect and PLGA, only a few signals were observed, demonstrating that the transplanted cell could promote the process of bone tissue regeneration. In summary, PMEV/BV not only constantly produced BMP2/VEGF to promote osteogenesis but also directly contributed to new bone formation by host cells. A significant advantage of this scaffold containing ToMSCs are that live cells infiltrated not only the surface but also the interior of the scaffold. As a result, the scaffold autonomously supported collagen remodeling and bone formation without relying on cell migration from surrounding damaged tissue into the structure. Such homogenous cell distribution may cut down bone regeneration time and the osteogenesis in the center and edge regions occurred simultaneously as shown in radiological and histological analysis (Figs. 6 and 7).

3. Discussion

This study introduces a VD-incorporated PLGA scaffold with MH designed to optimize the ratio of gene-edited ToMSC-BMP2/VEGF for osteogenesis. Our research unveiled that utilizing two types of ToMSCs and optimizing cell ratios within the scaffolds can activate distinct intercellular signaling pathways attributed to the specific functions of both BMP2 and VEGF. The results indicated that at a ratio of 2:1 for ToMSC-BMP2 to ToMSC-VEGF, the multifunctional PMEV/BV could induce M2 polarization, stimulate osteogenesis and vascularization, and exert a synergistic effect without hindrance. The immune environment and protein overexpression fostered osteogenic differentiation of MSCs and facilitated bone tissue regeneration *in vivo*, highlighting their superiority over cell-free scaffolds and spotlighting the potential of genetically engineered cells using CRISPR/Cas9 in bone tissue regeneration. Furthermore, we demonstrated the long-term activity of BMP2/VEGF and the pivotal role of MSCs in bone regeneration through the upregulation of osteogenic and angiogenic gene expression and the detection of human-specific markers.

Utilizing CRISPR/Cas9 for gene editing provides advantages over methods involving direct protein delivery or viral-mediated overexpression of stem cells. However, one limitation compared to methods involving direct protein delivery or viral-mediated overexpression of proteins involved in tissue regeneration is the potential for reduced therapeutic efficacy. CRISPR/Cas9 offers precise and versatile gene-editing capabilities, but its efficiency may vary depending on the target cell type and the specific genetic locus being modified, leading to suboptimal gene editing efficiency and potentially limiting therapeutic effectiveness for tissue regeneration. Additionally, ensuring efficient delivery of CRISPR/Cas9 components to target tissues or cells while minimizing off-target effects remains a significant hurdle in developing and clinically translating CRISPR-based therapies for tissue regeneration. Moreover, investigating the long-term safety and stability of CRISPR-mediated genomic modifications in tissue regeneration therapies is essential, as potential off-target effects, unintended genomic alterations, and immune responses to CRISPR-Cas9 components could compromise the safety and efficacy of these therapies over time.

In conclusion, this study proposes an innovative engineering approach to promote bone regeneration through safe gene-editing of cells within biomaterials. By exploring the optimized ratio of gene-edited ToMSC-BMP2/VEGF within a VD-incorporated PLGA scaffold with MH, our research sheds light on multifaceted intercellular signaling pathways activated by BMP2 and VEGF. Despite challenges related to variable efficiency and delivery hurdles, our findings underscore the superior potential of genetically engineered cells using CRISPR/Cas9 for bone tissue regeneration. Furthermore, elucidating the long-term activity of BMP2/VEGF and the crucial role of MSCs in bone regeneration emphasizes the need for further exploration in tissue engineering.

4. Conclusions

In this study, we developed a multifunctional scaffold incorporating vitamin D into poly(lactic-co-glycolic acid) (PLGA) combined with CRISPR/Cas9-mediated BMP2/VEGF-overexpressed tonsil-derived mesenchymal stem cells (ToMSCs) for bone tissue regeneration. Our findings demonstrated that this innovative scaffold significantly enhances both osteogenic and angiogenic potential *in vitro* and *in vivo*. The incorporation of vitamin D into the PLGA scaffold not only improved its M2 polarization inductivity but also provided a sustained release that promotes osteogenic differentiation. The CRISPR/Cas9 technology allowed for the precise overexpression of BMP2 and VEGF in ToMSCs, leading to robust bone formation and improved vascularization, crucial for successful bone tissue engineering. Additionally, the immunomodulatory properties of the scaffold, evidenced by the favorable shift from M1 to M2 macrophages, suggest its potential to create a conducive environment for tissue regeneration by mitigating inflammation. Despite the promising results, it is essential to acknowledge the limitations of this study, including the need for long-term studies to assess the scaffold's efficacy and safety in more complex *in vivo* models and the evaluation of potential immunogenic responses. Future research should aim to optimize the scaffold's composition and thoroughly investigate its long-term effects in preclinical and clinical settings.

5. Materials and methods

5.1. Materials

PLGA (lactide:glycolide = 50:50, M_w = 150 kDa) was purchased from Evonik Ind. (Germany). Magnesium hydroxide (MH) and VD were purchased by Sigma-Aldrich (USA). The bovine bone-derived extracellular matrix powder (bECM) was supplied by Oscotec Inc. (Korea). Matrigel matrix was purchased from Corning Life Sciences (USA).

5.2. Isolation and culture of tonsil-derived mesenchymal stem cells

FACS analysis demonstrated expression of CD44, CD73, CD90, CD105, HLA-DRB1, and HLA-ABC with ToMSCs (Supplementary Fig. 1). The isolated ToMSCs were differentiated into various cell lineage including adipocyte, osteocyte, and chondrocyte to confirm multipotency of the cells. Tonsil tissue was acquired from a five-year-old child who underwent a tonsillectomy at the Department of Otolaryngology, Bundang CHA Hospital (Korea). This procedure was conducted with the approval of the Institutional Review Board of Bundang CHA Hospital, under approval number 2021-03-016. The postoperative tonsil tissue underwent a thorough procedure: it was rinsed twice using phosphate-buffered saline (PBS; Welgene, Korea) solution, then carefully sliced

into small pieces with a sterile knife. Subsequently, it was subjected to digestion using 210 U/ml of collagenase type 1 (Invitrogen, Waltham, USA) and 10 μg/ml of DNase (Sigma-Aldrich) for 30 min at 37 °C. The digested tissue was then strained through a wire mesh, and the collected cells were washed twice with RPMI-1640/20 % fetal bovine serum (FBS; Gibco, USA), followed by an additional wash with RPMI-1640/10 % FBS. Mononuclear cells were obtained through density gradient centrifugation on Ficoll-Paque (GE Healthcare, UK). For the cultivation of these mononuclear cells, 1×10^8 cells were seeded into T-125 culture flasks containing Dulbecco's modified Eagle's medium Ham's F-12 nutrient mixture (DMEM F12, Thermo Fisher Scientific, USA), supplemented with 10 % FBS, 100 μg/ml streptomycin (Invitrogen), and 100 U/ml penicillin (Invitrogen). After 48 h, the non-adherent cells were removed, leaving behind the adherent cells, which were further expanded in fresh medium.

5.3. Flow cytometry for surface marker of ToMSCs

Flow cytometry was employed to characterize the phenotype of ToMSCs. A minimum of 10,000 cells, suspended in 100 μL of PBS solution containing 2 % FBS, were subjected to analysis with monoclonal antibodies targeting specific markers. These markers included positive markers APC-CD44, PE-CD73, PE-CD90, and APC-CD105 (all sourced from Miltenyi Biotec, Germany), as well as negative markers PE-HLA-DR (BD Biosciences, Franklin Lakes, USA) and FITC-anti-HLA-ABC (Thermo Fisher Scientific). ToMSCs underwent flow cytometric analysis using antibodies capable of recognizing several surface markers, including MSC-specific markers: Anti-CD44, Anti-CD73, Anti-CD90, and Anti-CD105 (all sourced from Miltenyi Biotec, Germany), in addition to Anti-HLA-DRB1 (BD Biosciences) and Anti-HLA-ABC (Thermo Fisher Scientific).

5.4. Plasmid construction

At first, a DNA fragment containing BMP2-6his, with *Sal*I and Mlu I sites situated at the 5′- and 3′-ends respectively, was synthesized via PCR. This PCR utilized pTetON-BMP2/BMP7 (Addgene, USA) as a template. Subsequently, the synthesized DNA fragment was cloned into a pTA vector (Real Biotech Corp, Taiwan). The BMP2-6his DNA fragment was then isolated through a double digestion involving *Sal*I and Mlu I enzymes, after which it was inserted into a plasmid adeno-associated virus integration site 1 (pAAVS1)-puro-CAG-EGFP plasmid (Addgene) previously digested with *Sal*I and Mlu I enzymes. The AAVS1-puro-CAG-VEGFA-6his plasmid was constructed following the same methodology as the AAVS1-puro-CAG-BMP2-6his plasmid. In this instance, the VEGFA-6his DNA fragment was generated through PCR, employing pGEM-T VEGFA (Korea Human Gene Bank, Korea) as a template.

5.5. CRISPR/Cas9-mediated knock-in gene editing

The CRISPR/Cas9 system has been employed to insert gene cassettes into a secure genomic locus known as the AAVS1 [37,38]. The transfection of ToMSCs (passage 1) was carried out using the Neon™ transfection system (Invitrogen) at 990 V, 40 ms, with 2 pulses. The knock-in conditions included 6.25 μg of Cas9 protein, 12 μg of sgRNA, and 1 μg of donor DNA. The donor DNA utilized in this study comprised AAVS1-Puro-CAG-BMP2-6his and AAVS1-Puro-CAG-VEGFA-6his. Following electroporation, cells were subjected to puromycin selection (0.8 μg/ml, Sigma-Aldrich) between 48 and 72 h to identify successfully modified colonies. Subsequently, selected clones were maintained in the presence of 0.16 μg/ml puromycin. The Cas9 protein was procured from CosmoGenetech (Korea).

6. Immunocytochemistry

Cells were first rinsed with ice-cold PBS solution and subsequently fixed with 4 % paraformaldehyde in PBS solution (Biosolution, Korea). After fixation, the cells were thoroughly washed four times with PBS solution and permeabilized for 10 min using 0.1 % Triton-X (Sigma-Aldrich). Following permeabilization, the cells were blocked using 5 % normal goat serum (NGS) (Thermo Fisher Scientific) and then incubated with primary antibodies overnight at 4 °C with gentle agitation. The primary antibodies used were anti-His tagged antibodies (1:2000) (ABM in Richmond, Canada) which were specific for ToMSC-BMP2-6his and ToMSC-VEGFA-6his. Following the overnight incubation with primary antibodies, the cells were washed three times with PBS solution and incubated with goat anti-rabbit AlexaFluor 594 IgG antibody (1:200) (Invitrogen) for 1 h at room temperature (RT). After an additional four washes with PBS solution, the cells were counterstained with 4′,6-diamidino-2-phenylindole, dihydrochloride (DAPI, 1:2000) (Sigma-Aldrich) and subsequently examined under a microscope.

6.1. In vitro differentiation of ToMSCs

For adipogenic differentiation, cells were seeded in a 12-well plate and cultured in adipogenic medium (Gibco) with regular medium changes every 3–4 days. After the 2 weeks period, the cells underwent a thorough rinse with PBS solution and were then fixed in 4 % paraformaldehyde for 15 min at RT. Following fixation, each well was stained with Oil Red O (Sigma-Aldrich) for 20 min at RT. For osteogenic differentiation, cells were seeded in a 12-well plate and were cultured in osteogenic culture medium (Gibco) with medium changes every 3–4 days. After these 3 week-culture periods, we removed the culture medium and rinsed the cells once with PBS solution. Subsequently, the cells were fixed using 60 % isopropyl alcohol for 5 min at RT. The cells were then stained with a 2 % Alizarin Red S solution (pH 4.2) (Sigma-Aldrich) for 10 min at RT. For chondrogenic differentiation, cells were seeded in a 12-well plate and cultured in chondrogenic culture medium (Gibco) with regular medium changes every 3–4 days. After 4-week culture period, we removed the culture medium, rinsed the cells with PBS solution, and then fixed them in 4 % paraformaldehyde. The cells were subsequently stained with a 1 % Alcian Blue 8GX solution (Sigma-Aldrich) for 30 min at RT. For adipocytes, the cells were washed with H_2O, and 1 ml of 100 % Isopropanol per well was added, followed by incubation for 10 min at RT. The resulting cell lysates were quantified using a microplate reader (TECAN, Switzerland) at a wavelength of 490 nm. For osteocytes, the cells were incubated with 1 ml/well of 10 % (w/v) cetylpyridinium chloride (Sigma-Aldrich) in 10 mM sodium phosphate for 30 min at RT. Subsequently, 100 μl of the cell lysates was analyzed at 550 nm. For chondrocytes, the cells were incubated in 4 M guanidinium HCl for 4 h at R/T. 100 μl of the cell lysates analyzed at 595 nm.

6.2. ELISA

The level of BMP2 protein secreted into the media by the cultured cells was measured using the Human BMP2 DuoSet ELISA kit (R&D Systems, USA), following the manufacturer's instructions. Likewise, for VEGFA, the level of VEGF protein secreted by the cells into the media was determined using the Human VEGF Quantikine ELISA kit (R&D Systems), also in accordance with the manufacturer's instructions.

6.3. Preparation of the PMEV scaffold

Modified MH with ricinoleic acid was synthesized by previous study [39]. The PLGA/MH/bECM/VD (PMEV) scaffold was fabricated by the freeze-drying method using a micro-ice particle, which has a size at 200–300 μm as a porogen. The modified MH (20 wt% compared to polymer) dissolved in 0.3 M dichloromethane solution was completely mixed with 0.5 g of PLGA. Then, 50 wt% bECM powder and 10 wt% VD were added to the above solution. All procedure was conducted at −20 °C. A 6.5 g of ice particles were added in the mixing solution and

stuffed into round PTFE mold (Φ5 x 2 mm^3). The porous scaffolds were obtained after 2 days for freeze drying to remove the porogen and remaining organic solvent.

6.4. Scaffold characterization

The surface morphology of the scaffold was visualized using scanning electron microscopy (SEM). The elemental mapping of the PMEV scaffold was executed using a FE-SEM equipped with energy dispersive spectroscopy (EDS). To measure the compressive modulus, universal testing machine (UTM) was performed with a capacity of 100 N load cell. The thermal property of each scaffold was analyzed by a thermogravimetric analyzer (TGA; TGA 4000, Perkin Elmer, Germany). The chemical structure of each scaffold and VD were evaluated by attenuated total reflectance-Fourier transform infrared (ATR-FTIR) spectroscopy (Perkin Elmer) on 600–4000 cm^{-1}. To assess the neutralization capacity of the scaffolds, the pH values were measured in 400 μl PBS solution for 49 days. The release profile of VD was evaluated with high performance liquid chromatography (HPLC, Vanquish VC-920-A, Thermo Fisher Scientific). The separation was carried out using Eclipse C18 reverse column 4.6 × 150 mm, 5 μm (Agilent, USA). The mobile phase was composed of 100 % methanol with a flow rate of 1 ml/min. A 10 μl of solution was injected into the column and detection was carried out at 265 nm for 5.8 min. Data collection and quantification were performed using Dionex Chromeleon 7 Chromatography Data system 7.3 software.

7. DPPH (2,2-diphenyl-1-picrylhydrazyl) ROS scavenging assay

The ROS scavenging ability of vitamin D was investigated using 2,2-diphenyl-1-picrylhydrazyl (DPPH). The PLGA, PM, PME, and PMEV scaffolds were added to the DPPH working solution (250 μM) at room temperature and protected from light. After 1 h, the absorbance of the DPPH solution was measured at 515 nm using a microplate reader. ROS scavenging ability was calculated by the following formula: DPPH absorbance (% of control) = [(Absorbance of scaffolds mixture)/(Average absorbance of control scaffold mixture)] x 100.

7.1. Flow cytometry analysis

RAW264.7 cells were seeded into 24 well plates for the M1/M2 polarization analysis. The next day, RAW264.7 cells were untreated or stimulated with IFN-γ (20 ng/ml, PeproTech, USA) and LPS (10 ng/ml, Sigma-Aldrich) for M1 polarization, and IL-4 (30 ng/ml, PeproTech) and IL-13 (30 ng/ml, PeproTech) for M2 polarization. Then, cells were incubated with scaffolds using 24 well inserts for 24 h. After 24 h cells were detached using accutase and washing with PBS solution. Cells were stained for 7-AAD viability staining solution for 5 min at 4 °C. The cells were washed with FACS buffer prior to incubation in fixation buffer at 4 °C for 10 min. The fixation cells were stained with CD86 (12-0862-82, eBioscience, USA), CD206 (141703, Biolegend, USA), and CD11b (17-0112-82, eBioscience) antibodies before performing the flow cytometry analysis. Finally, Flow Cytometry data were analyzed using CytExpert and FlowJo software.

7.2. Tube formation assay

Tube formation assay was conducted at precooled 24-well plate using Matrigel matrix with 1 ml of medium containing 1 % FBS. A 1.2 × 10^5 cells were seeded on 24-well plate, and the scaffolds were placed on hanging cell insert. After 24 h, HUVECs were stained with calcein AM (4 μmol; C1430, Thermo Fisher Scientific). The tube was quantified using ImageJ software for total tube length and number of branch point in each well.

7.3. Osteogenic differentiation

MC3T3-E1, mouse preosteoblast, were cultured in 24-well plate. After 1 day, the media were changed into an osteogenic differentiation medium containing 10 % FBS, 1 % antibiotic antimycotic, 50 μM L-ascobic acid, 10 nM dexamethasone, and 10 mM β-glycerophosphate. After 7 days, cells were fixed with 10 % formalin and rinsed with deionized water and stained with Takara ALP stain kit (MK300). The ALP activity was measured using ALP assay kit (MK301). All procedure were conducted according to the provided protocol. The alizarin red s (ARS; A5533) staining was executed to confirm mineralization of MC3T3-E1. After 14 days of osteogenic induction, ARS staining was conducted with 2 % solution. To quantify the mineralization, 10 % cetylpyridinium chloride (CPC; C0732, Sigma-Aldrich) was added to each well and incubated for 15 min to elute the calcium-bind alizarin red.

7.4. RNA extraction and RT-qPCR

RNA was extracted using Universal RNA Extraction Kit (K-3141, Bioneer, Korea) *in vitro* and TRIzol reagent (15596018) *in vivo* following the manufacturer's instructions. The RNA concentration was determined by a spectrophotometer (Nanodrop one, Thermo Fisher Scientific). Complementary DNA was synthesized using PrimeScript RT Reagent kit (Perfect Real Time, Takara). The RT-qPCR was performed using Power SYBR Green PCR Master Mix and QuantStudio 3 system (Applied biosystems, USA). The relative gene expressions were calculated with 18S rRNA as a reference gene. The RNA was extracted from the tissue at the site of the calvarial defect in SD rats for the RT-qPCR experiment.

7.5. Western blotting

The total protein of the cell and tissue was extracted by RIPA lysis buffer (#9806, Cell Signaling Technology). To investigate osteoinductive cytokines on MC3T3-E1, ToMSCs or ToMSC-BMP2 seeded scaffold was placed on hanging cell insert. The total protein was subjected to SDS-PAGE, transferred onto nitrocellulose membranes, and probed overnight at 4 °C with specific primary antibodies against as follows: RUNX2 (sc-390351, Santa cruz, 1:400). The angiogenic cytokines were investigated with ToMSCs or ToMSC-BMP2 seeded scaffold on HUVECs. The VEGF signaling pathway was probed with primary antibodies against as follows: p-Akt (AP0637, ABclonal, 1:2000), Akt (2920S, Cell Signaling Technology, 1:2000), p-MEK1/2 (AP1021, ABclonal, 1:2000), p-ERK1/2 (9101S, Cell Signaling Technology, 1:1000), ERK1/2 (sc-514302, Santa cruz, 1:400), β-actin (sc-47778, Santa cruz, 1:400). Horseradish peroxidase-conjugated anti-mouse (7076S, Cell Signaling Technology) and anti-rabbit (7074P2, Cell Signaling Technology) secondary antibodies were used with 1:5000 dilution.

7.6. In vivo surgical procedure

The experimental protocols for the use of animals were approved by the Institutional Animal Care and Use Committee of CHA University (IACUC230123). The 8 weeks-aged SD rats were used in this study. The animals were anesthetized with an isoflurane (Terrell Isoflurane, Piramal Critical Care Inc.). The hair was shaved, and the exposed skin was sterilized with ethanol. Then, a sagittal incision was executed. A 4 mm defect was made on both sides of the rat calvaria at a certain distance from the sagittal suture line using a micro drill. The periosteum was closed with absorbable sutures, and the epidermis of implanted site was sutured with nonabsorbable sutures. The vascularization of the defect was assessed using Microfil (MV-122, Flow Tech). After 8 weeks of implantation, the hair of the chest was shaved, and the ribs were opened using scissors. The left ventricle was penetrated during anesthesia with a 21-gauge butterfly needle, and then 50 ml of heparinized saline and 50

ml of 4 % paraformaldehyde were completely perfused at rate of 9 ml/min using Microfluidic Syringe pump (NE-1000-ES). Last, 20 ml of Microfil was perfused at a rate of 2 ml/min. The perfused samples were set overnight at 4 °C to completely cure the contrast agent.

8. Micro-CT for new bone formation and vascularization

The obtained rat calvarias were fixed with 4 % paraformaldehyde at 25 °C for 7 days for micro-CT scanning. Microfil-infilled samples were decalcified for 2 weeks using decalcifying solution (BBC 6089, BBC biochemical). Images were obtained at x-ray tube voltage, 90 kVp; x-ray tube current, 180 μA; and field of view (FOV), 20 mm using Quantum FX micro-CT (PerkinElmer). The bone volume density (BV/TV; %) and BMD (g/mm^3) were measured with the Analyze 12.0 (threshold, 5000∼; region of interest, 100 × 100 × 50).

8.1. Histological evaluation

All fixed and decalcified samples were embedded into paraffin and sectioned at 10 μm thickness. The sectioned slides were stained with Hematoxylin & Eosin (H&E; ab245880, Abcam) and Masson's Trichrome (MT; VitroView, VitroVivo Biotech). The immunostaining was conducted to detect expression of human-specific cell marker and BMP2/VEGF signaling molecules using antibody as follow: STEM121™ (Y40410, Takara; 1:200), p-ERK1/2 (1:200).

8.2. Statistical analysis

All experiments were repeated at least three times. The results are shown as means ± SEM. $\#p < 0.0001$, $***p < 0.001$, $**p < 0.01$, and $*p < 0.05$ indicate a statistically significant difference, respectively. Statistically significant differences were evaluated by one-way analysis of variance (ANOVA) using Tukey method in GraphPad Prism 9.0 software (GraphPad Software, USA).

CRediT authorship contribution statement

So-Yeon Park: Writing – original draft, Methodology, Investigation, Data curation, Conceptualization. **Jun-Kyu Lee:** Writing – review & editing, Supervision, Methodology, Formal analysis, Conceptualization. **Sang-Hyeok Lee:** Writing – original draft, Visualization, Validation, Investigation, Data curation. **Da-Seul Kim:** Writing – original draft, Visualization, Validation, Investigation, Data curation. **Ji-Won Jung:** Investigation, Data curation. **Jun Hyuk Kim:** Investigation, Data curation. **Seung-Woon Baek:** Investigation, Data curation. **Seungkwon You:** Supervision, Project administration. **Dong-Youn Hwang:** Writing – review & editing, Supervision, Project administration, Funding acquisition. **Dong Keun Han:** Writing – review & editing, Supervision, Project administration, Funding acquisition.

Declaration of competing interest

The authors declare that they have no known competing financial interests or personal relationships that could have appeared to influence the work reported in this paper.

Data availability

Data will be made available on request.

Acknowledgement

S-Y.P., J.-K.L., and S.-H.L. contributed equally to this work. This research was supported by the Korean Fund for Regenerative Medicine (KFRM) grant funded by the Korea government (the Ministry of Science and ICT, the Ministry of Health & Welfare) (2021M3E5E5095899 and 23A0206L1); and the Korea Medical Device Development Fund grant funded by the Korea government (the Ministry of Science and ICT, the Ministry of Trade, Industry and Energy, the Ministry of Health & Welfare, the Ministry of Food and Drug Safety) (Project Number: 1711196421, RS-2023-00255811), Republic of Korea.

Appendix A. Supplementary data

Supplementary data to this article can be found online at https://doi.org/10.1016/j.mtbio.2024.101254.

References

[1] B. Yuan, P. Liu, R. Zhao, X. Yang, Z. Xiao, K. Zhang, X. Zhu, X. Zhang, Functionalized 3D-printed porous titanium scaffold induces in situ vascularized bone regeneration by orchestrating bone microenvironment, J. Mater. Sci. Technol. 153 (2023) 92–105.
[2] T. He, H. Chen, P. Liu, H. Shi, X. Xu, C. Feng, Y. Wang, X. Li, N. Lei, Y. Xiao, X. Zhu, J. Xu, X. Zhang, One-step co-doping of ZnO and Zn2+ in osteoinductive calcium phosphate ceramics with synergistic antibacterial activity for regenerative repair of infected bone defect, J. Mater. Sci. Technol. 163 (2023) 168–181.
[3] C. Black, D. Gibbs, J. McEwan, J. Kanczler, M.P. Fernández, G. Tozzi, J. Dawson, R. Oreffo, Comparison of bone formation mediated by bone morphogenetic protein delivered by nanoclay gels with clinical techniques (autograft and InductOs®) in an ovine bone model, J. Tissue Eng. 13 (2022).
[4] H.Y. Lee, D.-S. Kim, G.Y. Hwang, J.-K. Lee, H.-L. Lee, J.-W. Jung, S.Y. Hwang, S.-W. Baek, S.l. Yoon, Y. Ha, K.N. Kim, I. Han, D.K. Han, C.K. Lee, Multi-modulation of immune-inflammatory response using bioactive molecule-integrated PLGA composite for spinal fusion, Mater. Today Bio 19 (2023) 100611.
[5] J.-K. Lee, D.-S. Kim, S.-Y. Park, S.-W. Baek, J.-W. Jung, T.-H. Kim, D.K. Han, Nitric oxide-Releasing bioinspired scaffold for exquisite regeneration of osteoporotic bone via regulation of homeostasis, Adv. Sci. 10 (2023) 2205336.
[6] D.-S. Kim, J.-K. Lee, J.H. Kim, J. Lee, D.S. Kim, S. An, S.-B. Park, T.-H. Kim, J. S. Rim, S. Lee, D.K. Han, Advanced PLGA hybrid scaffold with a bioactive PDRN/BMP2 nanocomplex for angiogenesis and bone regeneration using human fetal MSCs, Sci. Adv. 7 (2021) eabj1083.
[7] J.G. Werny, K. Sagheb, L. Diaz, P.W. Kämmerer, B. Al-Nawas, E. Schiegnitz, Does vitamin D have an effect on osseointegration of dental implants? A systematic review, Int. J. Implant Dent. 8 (2022) 16.
[8] D.-S. Kim, J.H. Kim, S.-W. Baek, J.-K. Lee, S.-Y. Park, B. Choi, T.-H. Kim, K. Min, D. K. Han, Controlled vitamin D delivery with injectable hyaluronic acid-based hydrogel for restoration of tendinopathy, J. Tissue Eng. 13 (2022) 20417314221122089.
[9] S.-Y. Oh, Y.M. Choi, H.Y. Kim, Y.S. Park, S.-C. Jung, J.-W. Park, S.-Y. Woo, K.-H. Ryu, H.S. Kim, I. Jo, Application of tonsil-derived mesenchymal stem cells in tissue regeneration: concise review, Stem Cell. 37 (2019) 1252–1260.
[10] H.-Y. Kim, H.-S. Yoon, Y. Lee, Y.-H. Kim, K.-A. Cho, S.-Y. Woo, H.S. Kim, K.-H. Ryu, J.-W. Park, Matrix metalloproteinase 1 as a marker of tonsil-derived mesenchymal stem cells to assess bone marrow cell migration, Tissue Eng. Regen. Med. 20 (2023) 271–284.
[11] P.K.F. Damasceno, T.A. de Santana, G.C. Santos, I.D. Orge, D.N. Silva, J. F. Albuquerque, G. Golinelli, G. Grisendi, M. Pinelli, R. Ribeiro dos Santos, M. Dominici, M.B.P. Soares, Genetic engineering as a strategy to improve the therapeutic efficacy of mesenchymal stem/stromal cells in regenerative medicine, Front. Cell Dev. Biol. 8 (2020) 737.
[12] J.A. Doudna, E. Charpentier, The new frontier of genome engineering with CRISPR-Cas9, Science 346 (2014) 1258096.
[13] H. Wang, M. La Russa, L.S. Qi, CRISPR/Cas9 in genome editing and beyond, Annu. Rev. Biochem. 85 (2016) 227–264.
[14] H. Lin, Y. Tang, T.P. Lozito, N. Oyster, B. Wang, R.S. Tuan, Efficient in vivo bone formation by BMP-2 engineered human mesenchymal stem cells encapsulated in a projection stereolithographically fabricated hydrogel scaffold, Stem Cell Res. Ther. 10 (2019) 254.
[15] Y. Zhang, Y. Han, Y. Peng, J. Lei, F. Chang, Bionic biphasic composite scaffolds with osteochondrogenic factors for regeneration of full-thickness osteochondral defects, Biomater. Sci. 10 (2022) 1713–1723.
[16] Q. Ma, Z. Miri, H.J. Haugen, A. Moghanian, D. Loca, Significance of mechanical loading in bone fracture healing, bone regeneration, and vascularization, J. Tissue Eng. 14 (2023) 20417314231172573.
[17] L. Polo-Corrales, M. Latorre-Esteves, J.E. Ramirez-Vick, Scaffold design for bone regeneration, J. Nanosci. Nanotechnol. 14 (2014) 15–56.
[18] H.A. Zaharin, A.M.A. Rani, F.I. Azam, T.L. Ginta, N. Sallih, A. Ahmad, N.A. Yunus, T.Z.A. Zulkifli, Effect of unit cell type and pore size on porosity and mechanical behavior of additively manufactured Ti6Al4V scaffolds, Materials 11 (2018) 15.
[19] S. Ma, X. Feng, F. Liu, B. Wang, H. Zhang, X. Niu, The pro-inflammatory response of macrophages regulated by acid degradation products of poly(lactide-co-glycolide) nanoparticles, Eng. Life Sci. 21 (2021) 709–720.
[20] J.S. Adams, M. Hewison, Update in vitamin D, J. Clin. Endocrinol. Metab. 95 (2010) 471–478.
[21] S. Zhou, M. Xie, J. Su, B. Cai, J. Li, K. Zhang, New insights into balancing wound healing and scarless skin repair, J. Tissue Eng. 14 (2023).

[22] S.Y. Chae, R. Park, S.W. Hong, Surface-mediated high antioxidant and anti-inflammatory effects of astaxanthin-loaded ultrathin graphene oxide film that inhibits the overproduction of intracellular reactive oxygen species, Biomater. Res. 26 (2022) 30.
[23] Y. Zhu, H. Liang, X. Liu, J. Wu, C. Yang, T.M. Wong, K.Y.H. Kwan, K.M.C. Cheung, S. Wu, K.W.K. Yeung, Regulation of macrophage polarization through surface topography design to facilitate implant-to-bone osteointegration, Sci. Adv. 7 (2021) eabf6654.
[24] L. Liang, D. Song, K. Wu, Z. Ouyang, Q. Huang, G. Lei, K. Zhou, J. Xiao, H. Wu, Sequential activation of M1 and M2 phenotypes in macrophages by Mg degradation from Ti-Mg alloy for enhanced osteogenesis, Biomater. Res. 26 (2022) 17.
[25] S. Han, X. Bao, Y. Zou, L. Wang, Y. Li, L. Yang, A. Liao, X. Zhang, X. Jiang, D. Liang, Y. Dai, Q.-C. Zheng, Z. Yu, J. Guo, d-lactate modulates M2 tumor-associated macrophages and remodels immunosuppressive tumor microenvironment for hepatocellular carcinoma, Sci. Adv. 9 (2023) eadg2697.
[26] Q. Zhang, B. Chen, F. Yan, J. Guo, X. Zhu, S. Ma, W. Yang, Interleukin-10 inhibits bone resorption: a potential therapeutic strategy in periodontitis and other bone loss diseases, BioMed Res. Int. 2014 (2014) 284836.
[27] S. Dichtl, L. Lindenthal, L. Zeitler, K. Behnke, D. Schlösser, B. Strobl, J. Scheller, K. C. El Kasmi, P.J. Murray, Lactate and IL6 define separable paths of inflammatory metabolic adaptation, Sci. Adv. 7 (2021) eabg3505.
[28] W. Shi, A.R.M. Fuad, Y. Li, Y. Wang, J. Huang, R. Du, G. Wang, Y. Wang, T. Yin, Biodegradable polymeric nanoparticles increase risk of cardiovascular diseases by inducing endothelium dysfunction and inflammation, J. Nanobiotechnol. 21 (2023) 65.
[29] W. Nimlamool, S. Potikanond, J. Ruttanapattanakul, N. Wikan, S. Okonogi, S. Jantrapirom, P. Pitchakarn, J. Karinchai, Curcuma amarissima extract activates growth and survival signal transduction networks to stimulate proliferation of human keratinocyte, Biol. (2021) 289.
[30] S.-Y. Wei, T.-H. Chen, F.-S. Kao, Y.-J. Hsu, Y.-C. Chen, Strategy for improving cell-mediated vascularized soft tissue formation in a hydrogen peroxide-triggered chemically-crosslinked hydrogel, J. Tissue Eng. 13 (2022).
[31] V. Asati, D.K. Mahapatra, S.K. Bharti, PI3K/Akt/mTOR and Ras/Raf/MEK/ERK signaling pathways inhibitors as anticancer agents: structural and pharmacological perspectives, Eur. J. Med. Chem. 109 (2016) 314–341.
[32] F. Peng, L. Qiu, M. Yao, L. Liu, Y. Zheng, S. Wu, Q. Ruan, X. Liu, Y. Zhang, M. Li, P. K. Chu, A lithium-doped surface inspires immunomodulatory functions for enhanced osteointegration through PI3K/AKT signaling axis regulation, Biomater. Sci. 9 (2021) 8202–8220.
[33] G. Lu, Y. Xu, Q. Liu, M. Chen, H. Sun, P. Wang, X. Li, Y. Wang, X. Li, X. Hui, E. Luo, J. Liu, Q. Jiang, J. Liang, Y. Fan, Y. Sun, X. Zhang, An instantly fixable and self-adaptive scaffold for skull regeneration by autologous stem cell recruitment and angiogenesis, Nat. Commun. 13 (2022) 2499.
[34] M.S. Rahman, N. Akhtar, H.M. Jamil, R.S. Banik, S.M. Asaduzzaman, TGF-β/BMP signaling and other molecular events: regulation of osteoblastogenesis and bone formation, Bone Res. 3 (2015) 15005.
[35] P. Carmeliet, R.K. Jain, Angiogenesis in cancer and other diseases, Nature 407 (2000) 249–257.
[36] K.V. Brown, B. Li, T. Guda, D.S. Perrien, S.A. Guelcher, J.C. Wenke, Improving bone formation in a rat femur segmental defect by controlling bone morphogenetic protein-2 release, Tissue Eng. 17 (2011) 1735–1746.
[37] J.R. Smith, S. Maguire, L.A. Davis, M. Alexander, F. Yang, S. Chandran, C. ffrench-Constant, R.A. Pedersen, Robust, persistent transgene expression in human embryonic stem cells is achieved with AAVS1-targeted integration, Stem Cell. 26 (2008) 496–504.
[38] D. Hockemeyer, F. Soldner, C. Beard, Q. Gao, M. Mitalipova, R.C. DeKelver, G. E. Katibah, R. Amora, E.A. Boydston, B. Zeitler, X. Meng, J.C. Miller, L. Zhang, E. J. Rebar, P.D. Gregory, F.D. Urnov, R. Jaenisch, Efficient targeting of expressed and silent genes in human ESCs and iPSCs using zinc-finger nucleases, Nat. Biotechnol. 27 (2009) 851–857.
[39] E. Lih, C.H. Kum, W. Park, S.Y. Chun, Y. Cho, Y.K. Joung, K.-S. Park, Y.J. Hong, D. J. Ahn, B.-S. Kim, T.G. Kwon, M.H. Jeong, J.A. Hubbell, D.K. Han, Modified magnesium hydroxide nanoparticles inhibit the inflammatory response to biodegradable poly(lactide-co-glycolide) implants, ACS Nano 12 (2018) 6917–6925.